Second-Harmonic Generation of Electron-Bernstein Waves in an Inhomogeneous Plasma

Nong Xiang[1,*] and John R. Cary[1,2]

[1]*Center for Integrated Plasma Studies, University of Colorado at Boulder, Boulder, Colorado 80309, USA*
[2]*Tech-X Corporation, Boulder, Colorado 80303, USA*

(Received 30 November 2007; published 27 February 2008)

In the injection of electron-Bernstein waves (EBW) into a plasma, proposed for plasma heating and current drive in over-dense plasma, conversion of the fundamental to its second harmonic is predicted analytically and observed in computations. The mechanism is traced to the existence of locations where one can have both wave number and frequency matching between the fundamental and its harmonic. Further, at such locations, the second harmonic commonly has minimal group velocity, and this allows the amplitude of the second harmonic to build to values exceeding that of the fundamental at power levels less than anticipated in experiments. The second-harmonic power can then be deposited at half-harmonic resonances of the original wave, often far from the desired location of energy deposition. Estimates for the power at which this is significant are given.

DOI: 10.1103/PhysRevLett.100.085002 PACS numbers: 52.35.Mw, 52.65.Rr

In over-dense plasma, where the plasma frequency is some multiple of the electron cyclotron frequency, electromagnetic waves at a low multiple of the cyclotron frequency cannot penetrate to the center of the plasma, where it is desired that the energy be deposited. However, conversion of the extraordinary (X) or ordinary (O) modes to an electron-Bernstein wave (EBW) has been identified [1–5] as a way to get rf energy into an over-dense plasma. For sufficiently steep density gradient [3] and frequency not too far from the second harmonic [6], a cutoff-resonance-cutoff triplet can lead to 100% conversion of incoming electromagnetic waves to electron-Bernstein modes, which ultimately deposit the energy and momentum into the plasma interior. But with the linear analysis well in hand, it is pressing to understand whether nonlinear effects can lead to any limitations. In this Letter, we show that nonlinear effects can lead to strong second-harmonic generation, so strong that much of the incoming wave energy is converted to an EBW on a higher-frequency branch. Moreover, in these cases, the energy is deposited at half-harmonic resonances of the original wave, which are typically at very different locations from the fundamental.

Nonlinear effects in Bernstein mode propagation have previously been studied. Parametric decay is known to occur from both theoretical and experimental studies [7–9]. In parametric decay, the incoming *pump* wave with frequency ω_0 and wave vector k_0 transfers its energy to two daughter waves at (k_1, ω_1) and (k_2, ω_2) with lower frequencies. For this transfer to occur, the matching conditions, $\omega_0 = \omega_1 + \omega_2$ and $k_0 = k_1 + k_2$, must be satisfied. It has also been found that the self-interaction of the ion Bernstein waves can give rise to a virtual, nonpropagating wave (or quasimode) at a harmonic frequency [10–12]. This quasimode can then transfer energy to the particles at half-harmonic cyclotron frequencies.

The process considered here differs from both the above cases. Unlike the first case, the frequency is upshifted; the energy in the fundamental, with (k_f, ω_f) is converted to a mode at twice the original frequency, i.e., one with ($k_h = 2k_f$, $\omega_h = 2\omega_f$). Unlike the second case, the conversion is to a propagating mode, which can carry the energy and momentum to another location. Furthermore, the process described here differs from dispersionless harmonic generation [13], where the harmonics copropagate. Finally, our case differs in that spatial inhomogeneity is critical to the process. With spatial inhomogeneity, there is typically a point where the matching can occur, and because the group velocity of the harmonic is typically small near that point, large energy transfer occurs.

Figure 1 illustrates how frequency and wave number matching occurs in EBW harmonic generation for various values of the ratio ω_{pe}/Ω_e of electron plasma frequency to electron gyrofrequency. The matching condition can be written as the two conditions $\omega_h/k_h = \omega_f/k_f$; i.e., the waves have the same phase velocity, and $\omega_h/\omega_f = 2$. The first condition says that the two points in k-ω space lie on a line passing through the origin. For a vertical line, the ratio of frequencies of the third branch to the first

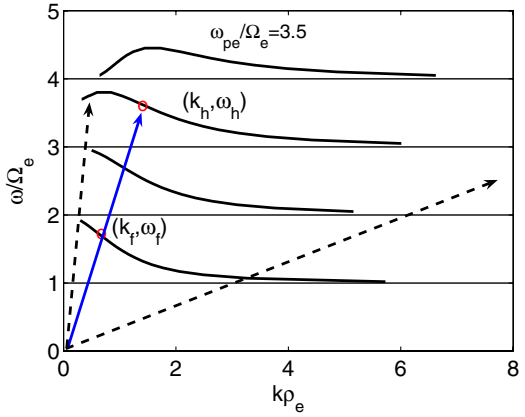

FIG. 1 (color online). Dispersion curves of EBWs for $\omega_e/\Omega_e = 3.5$.

 © 2008 The American Physical Society

branch is less than 2, while as the slope goes to zero, the ratio approached 3. Thus, there is a solution at intermediate phase velocity where the ratio is 2 and matching to the second harmonic can occur.

To reveal the second harmonic generation in a real space, we take the computational domain as: simulation size $L_x = 0.3$ m. The density given by $n_p(x) = n_c\{1 - \cos[\pi(x - x_{\rm edge})/(L_x - x_{\rm edge})]\}/2$, where $x_{\rm edge} = 0.1$ m and $n_c = 1.8 \times 10^{18}$ m^{-3}. Electron temperature $T_e \sim 200$ eV, magnetic field $B = 0.05$ T, incident frequency $f_0 \sim 2.5$ GHz. The density and frequency profiles are shown in Fig. 2.

Figure 3 shows the corresponding dispersion curves in phase space (k_x, ω). Plotted are $k_f(x, \omega)$, $2k_f(x, \omega)$, and $k_h(x, 2\omega)$. Where the crossing of the dashed and dotted lines occurs, one has matching, i.e., $2k_f(x, \omega) = k_h(x, 2\omega)$, and potentially strong transfer.

To estimate the power level at which second-harmonic generation occurs, we consider the mode coupling equation [14],

$$\frac{\partial(\omega_h \varepsilon_h)}{\partial k_h}\frac{\partial A_h}{\partial x} + \frac{1}{2}\frac{\partial}{\partial x}\left[\frac{\partial(\omega_h \varepsilon_h)}{\partial k_h}\right]A_h = M_h A_f^2 \qquad (1)$$

for plasma inhomogeneous in the x direction. In this equation, $\varepsilon_h = \varepsilon(\omega_h, k_h)$ is the dielectric function. A_h and A_f are the wave amplitude of the fundamental and harmonic, respectively. The coupling coefficient M_h is given by

$$M_h = \frac{\omega_e^2 \omega_h}{\Omega_e^2}\frac{q_e}{m_e k_h V_t^2} U(k_f, \omega_f)\langle e^{i(2\psi_f - \psi_h)}\rangle, \qquad (2)$$

with the bracket being a local spatial average. In this equation, the wave phases are $\psi_f = \int_{x_c}^{x} k_f dx'$, and $\psi_h = \int_{x_c}^{x} k_h dx'$, where x_c is the position where the resonant coupling takes place. In practice, the local spatial average is not needed, as upon integration in space, non resonant regions, where that term is highly oscillatory, give no net contribution to the integral. The expression for $U(k_f, \omega_f)$ will be presented elsewhere. We find numerically for our parameters that $U \sim 0.5$, and so $(\omega_e^2/\Omega_e^2)U \geq 1$ for our over-dense plasmas. In addition, the coupling typically occurs where the wave number $k_h(2\omega)$ is rapidly rising, and so the first and second terms in Eq. (1) are comparable. Hence, we can estimate using the second term, for which we use $\partial^2(\omega_h \varepsilon_h)/\partial x \partial k_h \sim \omega_h/(kL_n)$. One thus obtains

$$\frac{A_h}{L_n} \approx \frac{q_e}{m_e V_t^2} A_f^2. \qquad (3)$$

So as the pump field $A_f > m_e V_t^2/(q_e L_n)$, by Eq. (3), the field of the second-harmonic EBW will exceed the fundamental EBW. The corresponding value of the power is $\hat{P} \sim 0.5 n_e T_e (\lambda_D/L_n)^2 \omega(\partial\varepsilon/\partial k) S$, where S is the cross sectional area of the incoming radiation. We consider the parameters for proposed EBW experiments on the National Spherical Torus Experiment (NSTX), near the plasma edge, where $n_e \sim 5 \times 10^{17}$ m^{-3}, $T_e \sim 200$ eV, $B = 0.2$ T, $f_0 \sim 12$ GHz, $L_n \sim 0.4$ m, and $S \sim 0.0036$ m^{-3} for an S-band waveguide. Hence, $\hat{P}h \sim 40$ kW, less than planned values of 75 or so kW.

Computer simulations using the VORPAL [15] computational framework illustrate this process and allow accurate computations time and the field values at which harmonic generation occurs. Our simulations were two-dimensional, with x the direction into the plasma and y (the direction along the static magnetic field) being the second simulated direction. The nonsimulated direction, z, is the vertical direction, equivalent to the poloidal direction in toroidal geometry. The incident (X) wave is linearly polarized in the z direction and has the form $E_z(x = 0) = E_0(1 - e^{-\alpha t})^2 \sin(\omega_0 t)$, with $\alpha = 0.02\omega_0$ and $E_0 = 4 \times 10^4$ V/m. The ratio of the incident wave energy density and the electron thermal energy density near the funda-

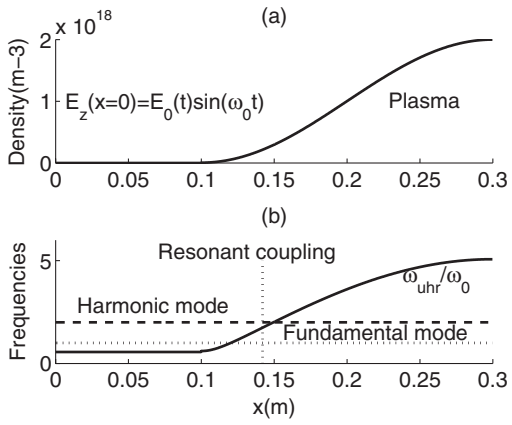

FIG. 2. (a) Simulation model and the plasma density profile, (b) normalized frequencies with the resonant coupling layer indicated.

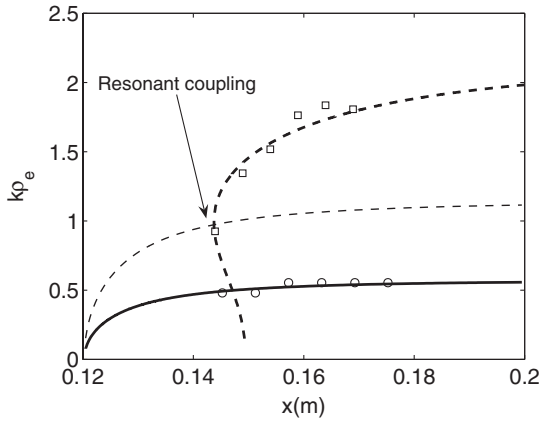

FIG. 3. EBW dispersion curves $k(x, \omega)$ (solid line), $2k(x, \omega)$ (light dashed line), and $k(x, 2\omega)$ (heavy dashed line). Circles are the measured values of k from the simulation for the fundamental. Squares the measure values of k from the simulation for the harmonic.

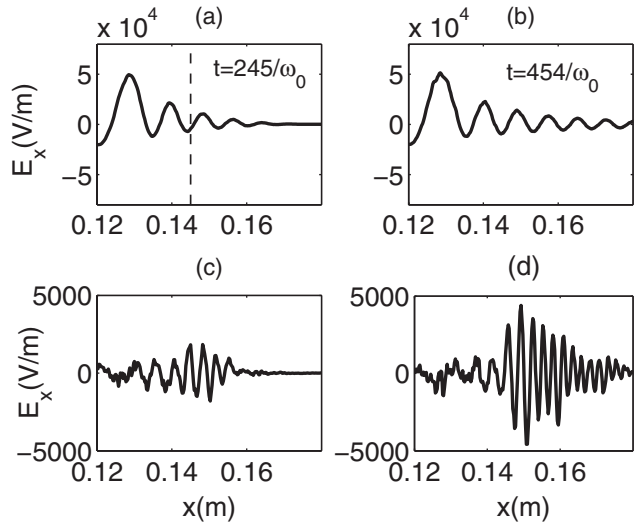

FIG. 4. Spatial distribution of the electrostatic fields (E_x) at the driving frequency [(a) and (b)] and its second harmonic [(c) and (d)] at $t = 245/\omega_0$ and $454/\omega_0$. The location of the resonant coupling is indicated in (a) by the dashed line.

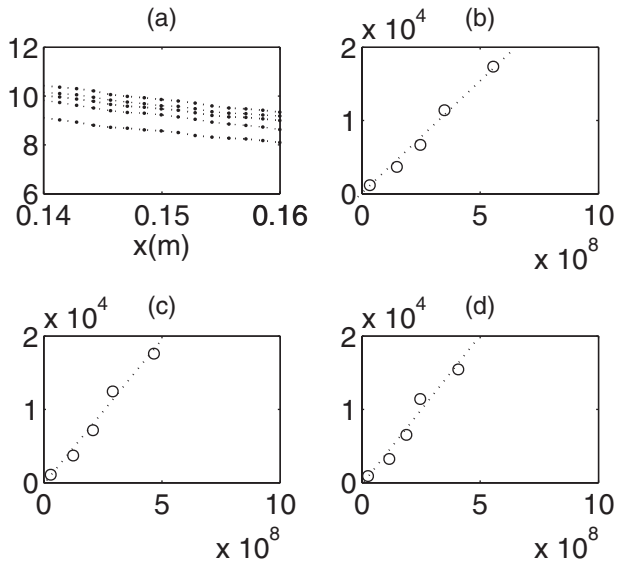

FIG. 5. (a) Logarithm of $|E_x|$ vs x at the driving frequency from different incident fields, $E_0 = 2 \times 10^4$, 4×10^4, 5×10^4, 6×10^4, and 8×10^4 V/m (from bottom to top). (b)–(c) show the amplitude of the second EBW vs the square of the amplitude of the fundamental EBW from the δf simulations (circles) at $x = 0.1456$ m, 0.1473 m, and 0.1489 m, respectively.

mental upper hybrid resonance (UHR) is about 0.02. To eliminate the noise issues of PIC at these parameters, the δf method [6,16,17] (an option in VORPAL) was used.

Second-harmonic generation was immediately apparent in the simulation. Through local Fourier analysis, we extracted the amplitudes at the first and second harmonics. These are shown in Fig. 4, where one sees that initially the second-harmonic amplitude is present around the coupling point $x \approx 0.145$ in Figs. 3 and 4. Later in time, the second harmonic grows and propagates into the plasma. Through spatially local Fourier analysis [6], we computed the local wave number for the perturbations. Those are plotted in Fig. 3 and agree well with theory.

The correct variation with power was seen through multiple simulations. These results are shown in Fig. 5. This figure shows that the incoming power decreases as it passes through the coupling point, and that the amplitude of the second harmonic at any one time is proportional to the square of the fundamental amplitude, as expected from Eq. (3).

The previous simulations were carried out with constant magnetic field to illustrate the process. However, for absorption, one must have a varying magnetic field so that the mode propagates to a resonance, where it is absorbed. In this case, the mode energy can end up deposited at a different location. As seen in Fig. 1, if the magnetic field increases as the incident wave propagates into the plasma, the fundamental might be resonant at the cyclotron frequency; meanwhile, the second harmonic might have resonance at three times the cyclotron frequency. Thus, while the fundamental would deposit its energy at $\omega = \Omega_e$, the second harmonic deposits its energy at $2\omega = 3\Omega_e$ or $\Omega_e = 2/3\omega$, a different location.

To illustrate this effect, we carried out simulations as before except with a spatially varying magnetic field, such that the fundamental now is resonant at $x = 0.185$ m, and the field decreases to the left so that the resonance $\Omega_e = 2/3\omega$ occurs at $x = 0.12$ m, while the resonance $\Omega_e = 2\omega$ occurs farther in, at $x = 0.27$ m. The resulting phase space is shown in Fig. 6. This diagram shows a second-harmonic wave to the left of the resonance, $\Omega_e = 2/3\omega$. In addition, to the right of that resonance the second harmonic can propagate by being on one of the other branches of Fig. 1. The propagating mode between the $\Omega_e = 2/3\omega$

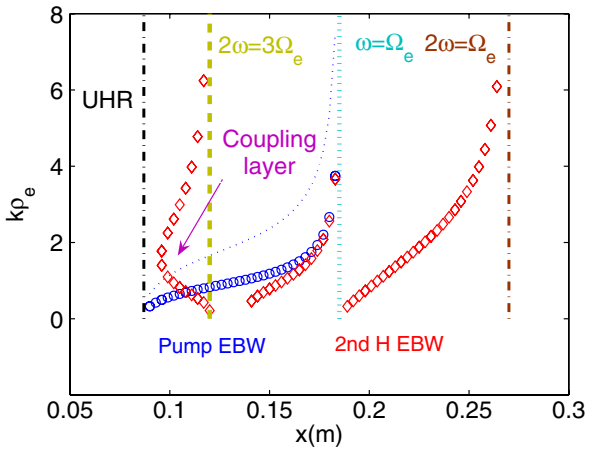

FIG. 6 (color online). Dispersion curves for pump EBW (circle) and second-harmonic EBW (diamond). The dotted line indicates the wave number twice the fundamental wave, and the cyclotron resonance layers are marked.

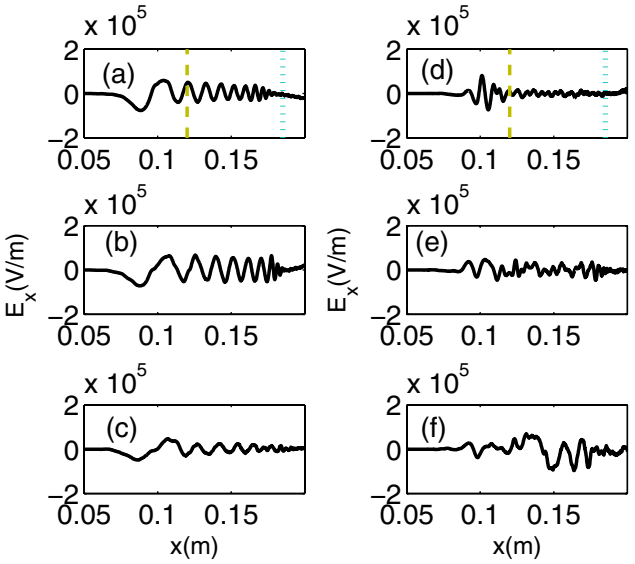

FIG. 7 (color online). Spatial distribution of the electrostatic fields (E_x) at the driving frequency [(a)–(c)] and its second harmonic [(d)–(f)] at $t = 252/\omega_0$, $532/\omega_0$, and $1405/\omega_0$, respectively. The cyclotron resonance layers $2\omega_0 = 3\Omega_e$ and $\omega_0 = \Omega_e$ are indicated in (a) and (d) by the dashed and dotted lines, respectively.

and the fundamental resonance corresponds to the second branch in Fig. 1, as it is twice the frequency and resonates at twice the gyrofrequency.

Figure 7 shows that indeed a second-harmonic field is generated outside the $\Omega_e = 2/3\omega$ resonance. This confirms that energy can be deposited in unexpected locations due to second-harmonic generation. Interestingly, there is significant harmonic generation at later times near the resonance of the fundamental. We expect that this is due to strong nonlinearities that are present at resonance and the fact that there is a propagating second harmonic at this location as well. In addition, the need for k-matching goes away, as the WKB approximation fails there.

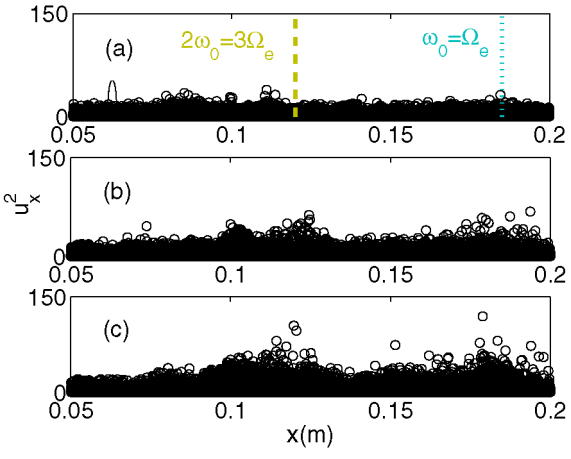

FIG. 8 (color online). Time history of $u_x^2 = (V_x/V_t)^2$ at (a) $t = 252/\omega_0$, (b) $532/\omega_0$, and (c) $1405/\omega_0$.

The heating is visible in Fig. 8 which plots the square of the velocity versus position. A caveat is that the heating in these simulations is much greater than it would be in an experiment, where the deposited energy spreads out poloidally and toroidally due to parallel transport. Nevertheless, this plot shows comparable deposition of energy at the expected resonance as well as the $3/2$ resonance of the second harmonic.

In summary, we have shown analytically and through computation that second-harmonic generations of electron-Bernstein waves in inhomogeneous plasmas can be significant at power levels planned for experiments, even though the power density is much smaller than plasma thermal energy density. Consequently, the amplitude of the harmonic mode can exceed the fundamental, and the wave power can end up absorbed at half electron cyclotron harmonic frequencies—at locations very different from what would expect otherwise. While not presented here, we mention that while this work concentrated on X-B mode conversion, we have seen some second-harmonic generation in O-X-B mode conversion as well, but more research is needed to understand the importance of second-harmonic generation in that process.

The work was supported by DOE Contract No. DE-FG02-04ER54735.

*xiangn@colorado.edu

[1] H. P. Laqua, V. Erkmann, H. J. Hartfuss, and H. Laqua, Phys. Rev. Lett. **78**, 3467 (1997).
[2] C. B. Forest, P. K. Chattopadhyay, R. W. Harvey, and A. P. Smirnov, Phys. Plasmas **7**, 1352 (2000).
[3] A. K. Ram and S. D. Schultz, Phys. Plasmas **7**, 4084 (2000).
[4] B. Jones, P. C. Efthimion, and G. Taylor *et al.*, Phys. Rev. Lett. **90**, 165001 (2003).
[5] G. Taylor, P. C. Efthimion, and B. Jones *et al.*, Phys. Plasmas **10**, 1395 (2003).
[6] N. Xiang, J. R. Cary, D. C. Barnes, and J. Carlsson, Phys. Plasmas **13**, 062111 (2006).
[7] R. P. H. Chang and M. Porkolab, Phys. Fluids **13**, 2766 (1970).
[8] M. Porkolab and R. P. H. Chang, Phys. Fluids **15**, 283 (1972).
[9] A. T. Lin and C.-C. Lin, Phys. Rev. Lett. **47**, 98 (1981).
[10] M. Porkolab, Phys. Rev. Lett. **54**, 434 (1985).
[11] R. Sugaya, Phys. Fluids **30**, 1730 (1987).
[12] M. Sugawa, Phys. Rev. Lett. **61**, 543 (1988).
[13] J. L. P. Mix, L. N. Litzenberge, and G. Bekefi, Phys. Fluids **15**, 2020 (1972).
[14] J. R. Cary and N. Xiang, Phys. Rev. E **76**, 055401 (2007).
[15] C. Nieter and J. R. Cary, J. Comput. Phys. **196**, 448 (2004).
[16] S. E. Parker and W. W. Lee, Phys. Fluids B **5**, 77 (1993).
[17] G. Hu and J. A. Krommes, Phys. Plasmas **1**, 863 (1994).